Tunable luminescence of Bi^{3+}-doped $YP_xV_{1-x}O_4$ ($0 \le x \le 1$)

2014 J. Phys.: Condens. Matter 26 385503

(http://iopscience.iop.org/0953-8984/26/38/385503)

OPEN ACCESS
IOP Publishing
Journal of Physics: Condensed Matter
J. Phys.: Condens. Matter **26** (2014) 385503 (13pp)
doi:10.1088/0953-8984/26/38/385503

Tunable luminescence of Bi^{3+}-doped $YP_xV_{1-x}O_4$ ($0 \leq x \leq 1$)

Enrico Cavalli[1], Fabio Angiuli[1], Francesco Mezzadri[1], Mattia Trevisani[2], Marco Bettinelli[2], Philippe Boutinaud[3] and Mikhail G Brik[4]

[1] Department of Chemistry, University of Parma, Parma, Italy
[2] Luminescent Materials Laboratory, Department of Biotechnology, University of Verona, and INSTM, UdR Verona, Verona, Italy
[3] Clermont Université, ENSCCF, Institut de Chimie de Clermont-Ferrand, Clermont-Ferrand, France
[4] Institute of Physics, University of Tartu, Ravila 14 C, Tartu 50411, Estonia

E-mail: enrico.cavalli@unipr.it

Received 10 June 2014, revised 23 July 2014
Accepted for publication 30 July 2014
Published 4 September 2014

Abstract

A systematic investigation of the luminescence spectroscopy of $Y(P,V)O_4:Bi^{3+}$ is presented. The emission spectra and the decay curves are measured as a function of the host morphology, composition, temperature, excitation wavelength, and doping concentration. On this basis, the nature of the excited states and the radiative and non-radiative relaxation processes are discussed. Colour coordinates and quantum yield measurements are also carried out to provide information about the potential applications of the studied materials.

Keywords: luminescence, Bi^{3+}, yttrium vanadate, yttrium phosphate

(Some figures may appear in colour only in the online journal)

1. Introduction

The luminescence of Bi^{3+} in oxide materials has been extensively investigated for a long time from both the applicative and the fundamental points of view [1–3]. In addition, the beneficial effect of Bi^{3+} co-doping on the luminescence performance of different lanthanide ions upon UV-blue excitation has been demonstrated in various host lattices, including YAG [4], YBO_3 [5], $CaTiO_3$ [6], YPO_4, YVO_4, and (in the last two cases) in their mixed phases [7–9]. The emission mechanisms in both singly and co-doped materials strongly depend on the interactions between the Bi^{3+} doping ions and the host lattice. In this context, YPO_4 and YVO_4 and their mixed phases constitute a good model system for the investigation of Bi^{3+} emission properties. They are, in fact, isostructural and have a single Y^{3+} site available for accommodation of Bi^{3+} and/or rare earth ions. The remainder have rather different physical and spectroscopic properties, as shown in table 1.

These properties will vary suitably along the mixed system. Old studies on the luminescence of $YPO_4:Bi^{3+}$ reported that this material emits at 330 nm upon 230 nm excitation [1, 15] whereas more recent VUV spectroscopy experiments [16] have revealed a strong emission band in the UV region at 240 nm. The yellow luminescence of $YVO_4:Bi^{3+}$ was investigated in the late 1960s [1] and ascribed to the formation of a charge transfer state between host and doping ions. The absorption and emission spectra and the energy transfer processes in YVO_4 and Bi^{3+}-doped YVO_4 are dealt with in [17]. However, a recent paper [18] has proposed an assignment in contrast with the previous literature, evidencing the opportunity of an updated survey of their spectroscopic properties. Starting from the end members of the $Y(P_xV_{1-x})O_4:Bi^{3+}$ series, we investigated their luminescence properties as a function of several parameters, including the host composition and excitation wavelength among others. The results were analyzed in the framework of a model recently proposed by Boutinaud [19] in which the Bi^{3+}-related yellow emitting state is identified with a metal-to-metal charge transfer (MMCT) state originating from the interaction of the doping ions with the vanadate host.

Table 1. Selected representative properties of the YPO_4 and YVO_4 host lattices.

	YPO_4	YVO_4
Bandgap (eV)	9.2 [10]	4.2 [13]
$\hbar\omega_{cutoff}$ (cm^{-1})	1070 [11]	890 [12]
Refractive index (av.)	1.75 [14]	2.02 [14]
Luminescence	No	Yes

The following empirical equation relates the position of the MMCT band with some host properties:

$$\mathrm{MMCT}(\mathrm{Bi}^{3+}, \mathrm{cm}^{-1}) = k_{CN'}\left[\chi_{CN}(\mathrm{Bi}^{3+}) - \alpha_{CN'}^{CN}\frac{\chi_{CN'}(\mathrm{M}^{n+})}{d_{corr}}\right] \quad (1)$$

where χ_{CN}(A) is the electronegativity of the *CN*-fold coordinated A ion (Bi^{3+} or the d^0 metal ion M^{n+}, V^{5+} in this case), d_{corr} is the shortest Bi^{3+}-M^{n+} interatomic distance corrected for the doping effect, and $k_{CN'}$ and $\alpha_{CN'}^{CN}$ are suitable structure-related quantities defined in [19]. In addition, we revisited some spectroscopic properties of the host lattices to better assess the role of excitation migration in emission dynamics.

2. Experimental methods

2.1. Synthesis and structural characterization

$Y_{1-y}(P_xV_{1-x})O_4$:Bi^{3+} (x = 0, 0.2, 0.5, 0.6, 0.7, 0.8, 1; y = 0, 0.001, 0.01) phosphors were synthesized by the sol-gel Pechini methodology described in previous papers [20, 21]. Pure YVO_4, Bi^{3+}-doped YVO_4, and $YP_{0.99}V_{0.01}O_4$ crystals up to 1 × 1 × 3 mm^3 in size were grown by the flux growth method [22, 23]. Powder XRD patterns were collected using Cu K_α radiation (λ= 1.541 78 Å) with a Thermo ARL X'tra powder diffractometer equipped with a Thermo Electron solid state detector. Data were collected in the 5°–90° 2θ range with 0.02° steps and 10 s of counting time. The morphology of the phosphors particles was examined by means of a Quanta 250 FEG scanning electron microscope (SEM).

2.2. Spectroscopic measurements

The 7 and 300 K emission and excitation spectra of YPO_4:Bi^{3+} were measured at the SUPERLUMI experimental station of HASYLAB (DESY, Germany) using the synchrotron radiation (SR) from the DORIS III storage ring as excitation source. For the measurement of excitation spectra in the range 3.7–19 eV, a 2 m monochromator in a McPherson mounting with a resolution of 3.2 Å was used. Detection of luminescence was performed with a 0.3 m ARC SpectraPro-308i monochromator equipped with a high-speed R3809U-50 S (Hamamatsu) microchannel plate detector. The excitation spectra were corrected for wavelength-dependent variation of the SR intensity using the sodium salicylate signal. Room temperature emission and excitation spectra were measured using a Fluoromax-3 (Jobin-Yvon) spectrofluorimeter. High resolution emission spectra were recorded down to 10 K using a spectroscopic system consisting of a 450 W Xe lamp fitted with a 0.2 m monochromator as source and a 1.26 m Spex monochromator with a RCA C31034 photomultiplier to analyze and detect the output radiation. The samples were mounted onto the cold finger of a He-cryocooler (Air Products Displex DE-202). The decay profiles were acquired in the temperature range 30–300 K using a HR1000 Jobin-Yvon monochromator, a R1104 Hamamatsu photomultiplier, and a 400 MHz Lecroy digital oscilloscope with an input impedance of 50 Ω. The samples were excited at 337 nm by a nitrogen laser or at 306.5 nm by means of the radiation generated by frequency doubling the output of a ND 60 dye laser operated with a Rhodamine 640 and pumped with a pulsed frequency doubled Nd:YAG laser. The quantum yield values and the trichromatic coordinates of all powders were measured at room temperature using the C9920-02G PL-QY measurement system from Hamamatsu. The setup comprised a 150 W monochromatized Xe lamp, an integrating sphere (Spectralon Coating, $\emptyset$ = 3.3 in.), and a high sensitivity CCD camera for detection of the whole spectral luminescence.

2.3. DFT calculations

The *ab-initio* analysis of the electronic structures of the host materials was carried out using experimental crystallographic data as input information. All calculations were performed in the density functional theory (DFT) framework as implemented in the CASTEP module [24] of Materials Studio. The plane wave basis set cut-off energy was set at 380 eV, the Monkhorst-Pack scheme k-point grid sampling was set as 3 × 3 × 3 k-points for the Brillouin zone for geometry optimization and 5 × 5 × 5 for electronic properties calculations. The convergence tolerance parameters were as follows: energy 5 × 10^{-6} eV/atom, maximal force and stress 0.01 eV/Å and 0.02 GPa, and maximal displacement 5 × 10^{-4} Å. The electronic configurations were $2s^22p^4$ for oxygen, $4d^15s^2$ for yttrium, $3s^23p^63d^34s^2$ for vanadium, and $3s^23p^3$ for phosphorus. After the crystal structures of the host materials were optimized (allowing for a complete relaxation of the ionic positions), the band structures and total and partial density of states (DOS) were calculated.

3. Results and discussion

3.1. Structure and morphology

The XRD patterns of the synthesized samples (figure 1(*a*)) confirm their zircon-type structure with the absence of impurity phases. The narrow peaks characterising the end-members of the series indicate that they have good crystallinity. YPO_4 and YVO_4 are isomorphic and form a complete solid solution. Their space group is $I4_1/amd$, with Z= 4. The tetrahedral vanadate ion is about 8% larger than the phosphate anion [25]. The peak broadening observed in the patterns of the solid solutions suggests the presence of disorder induced by the random distribution of the (VO_4) and (PO_4) units within the host lattice. As shown in [26], for the system $YP_xV_{1-x}O_4$:Eu^{3+}, this structural disorder impacted luminescence behaviours by modifying the local environment of the emitting ion. All the patterns shown in figure 1(*a*) were analyzed by the Rietveld method. The determined unit cell parameters and volume cells

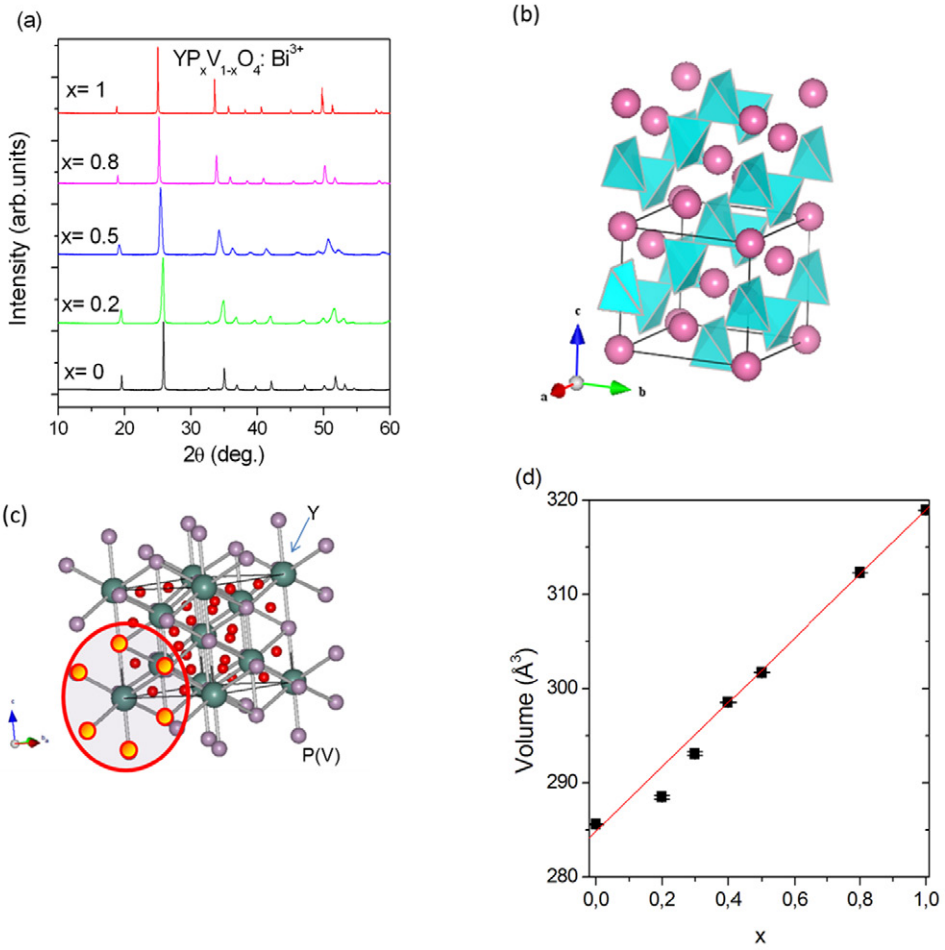

Figure 1. (*a*) Powder XRD patterns of the $YP_{1-x}V_xO_4$: Bi^{3+} series. (*b*) The zircon structure (elaborated using the VESTA software [28]). (*c*) Cation distribution in the second coordination sphere of Y(Bi). (*d*) Variation of cell volume with composition.

Table 2. Cell parameters (Å), cell volumes (Å^3), selected distances (Å), and Rietveld agreement factors in $Y(P_xV_{1-x})O_4$:Bi^{3+}.

x	a	c	V	Y-P(V)	R(F^2) (%)
1	6.8860(1)	6.0230(9)	285.61(7)	3.0116(3) x2 3.7579(3) x4	7.8
0.8	6.9053(2)	6.0500(9)	288.48(2)	3.0250(6) x2 3.7694(7) x4	9.1
0.5	6.9390(9)	6.0866(2)	293.10(1)	3.0433(8) x2 3.7885(8) x4	8.7
0.4	6.9765(3)	6.1336(5)	298.53(3)	3.0668(2) x2 3.8104(2) x4	10.8
0.3	6.9996(2)	6.1578(3)	301.70(2)	3.0789(1) x2 3.8234(1) x4	3.5
0.2	7.0729(1)	6.2427(1)	312.30(1)	3.1213(1) x2 3.8655(1) x4	4.2
0	7.1190(9)	6.2930(9)	318.93(1)	3.1463(1) x2 3.8917(1) x4	3.2

are listed in table 2 together with the Y-P(V) distances, which are useful in the interpretation of the spectroscopic results. They are consistent with the literature data [27]. The crystal building consists of chains of alternating edge-sharing $P(V)O_4$ tetrahedra and YO_8 units extending parallel to the crystallographic c axis (figure 1(*b*)). The Bi^{3+} doping ions replace Y^{3+} in dodecahedrally coordinated sites with nominal D_{2d} point symmetry. We note also that the second coordination sphere of $Y^{3+}(Bi^{3+})$ consists of two different kinds of $P^{5+}(V^{5+})$ ions located at distances of 3.01–3.15 Å (2 ions, axial position) and 3.75–3.89 Å (four ions, compressed tetrahedral arrangement), respectively (figure 1(*c*)). It is known that solid solutions of $YP_xV_{1-x}O_4$ can deviate appreciably from the Vegard's law depending on the preparation method [27].

In the present case, the volume cells follow Vegard's law reasonably well (figure 1(*d*)) and confirm the formation of the desired phases in agreement with previous studies [20].

The SEM images (figures 2(*a*)–(*c*)) reveal sub-micrometric sized grains with the rod-like shape typical of the zircon structure. The morphology did not change significantly on passing from the pure phosphate (figure 2(*a*)) to the pure vanadate (figure 2(*b*)) host and to the mixed phases (figure 2(*c*) as an example).

3.2. YPO_4:Bi^{3+}

The 7 K excitation and the 7 and 300 K emission spectra of YPO_4:Bi^{3+} (1%) are shown in figure 3(*a*). The excitation spectrum consists of an intense single band at 227 nm and of a composed system in the 150–190 nm region, both overlapping a baseline rising with increasing energy. They can be assigned

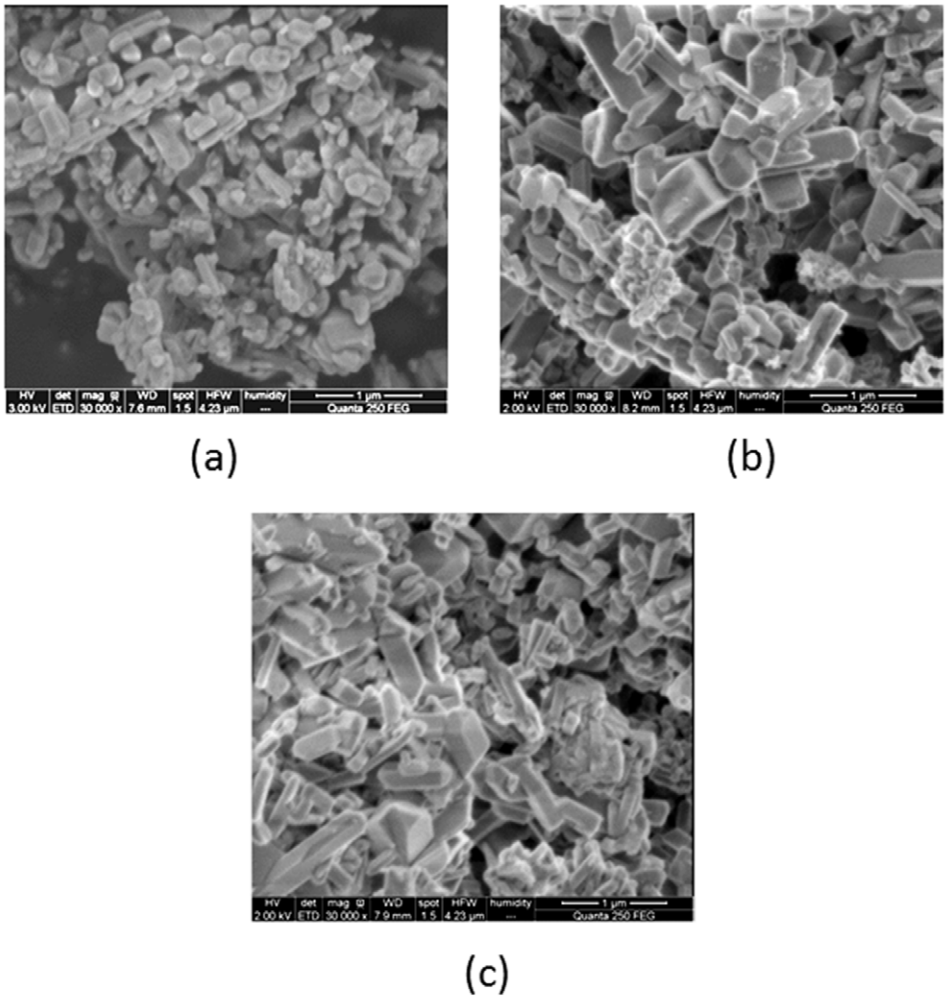

Figure 2. SEM images of YPO_4: Bi^{3+} (*a*), YVO_4: Bi^{3+} (*b*), and $YP_{0.5}V_{0.5}O_4$: Bi^{3+} (*c*).

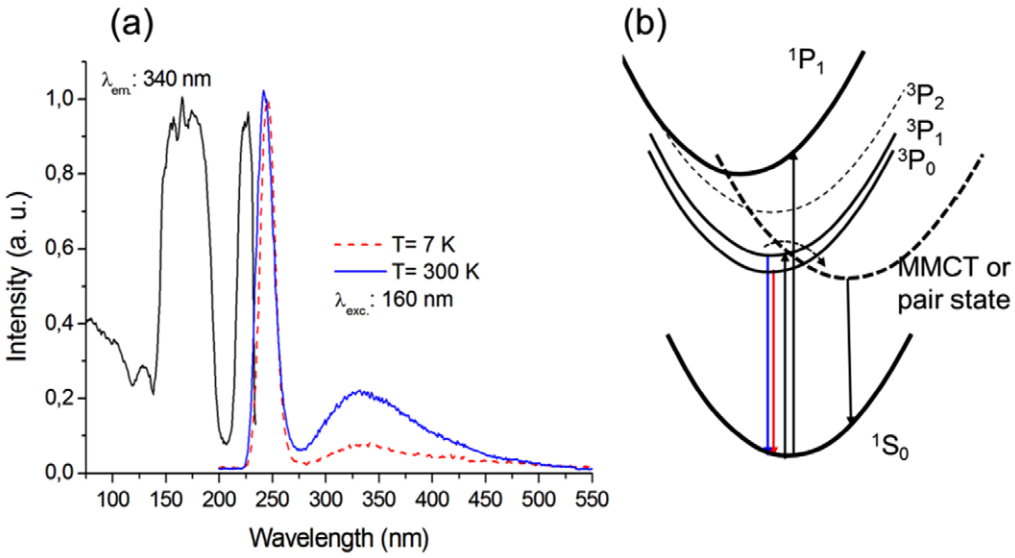

Figure 3. Time-integrated excitation and emission spectra of YPO_4:Bi^{3+} (*a*) and scheme of the involved dynamic processes (*b*).

to the $^3P_1 \leftarrow {}^1S_0$ and $^1P_1 \leftarrow {}^1S_0$ transitions of Bi^{3+}, respectively [1]. The emission is composed of an intense and sharp band pertaining to the isolated Bi^{3+} centre, peaking at 246 nm in the 7 K spectrum and at 243 nm in the 300 K spectrum. This shift is similar to that observed in a number of materials [29] and has been ascribed to the fact that at low temperatures,

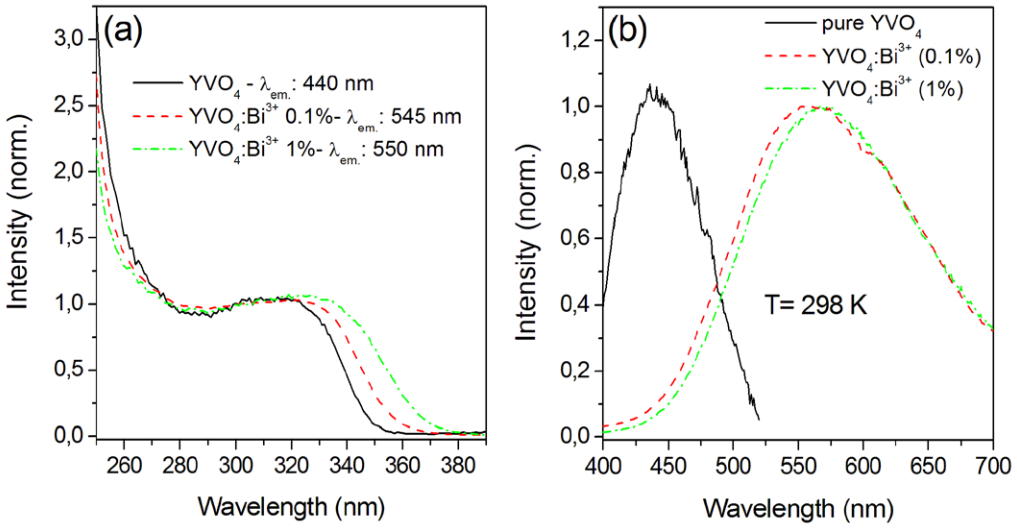

Figure 4. Room temperature excitation (*a*) and emission (*b*) spectra of YVO_4 and YVO_4:Bi^{3+}. The spectra are normalized with respect to the maximum emission.

the emission originates in the $^3P_0$ state whereas at room temperature it takes place from the thermally populated $^3P_1$ level, separated by about 500 cm^{-1} (0.06 eV) from $^3P_0$. A broadband extending from 280 to 450 nm with maximum at about 335 nm is also present. In the spectrum reported by Jüstel [16], this component was barely observable and not assigned. As the temperature is raised to 300 K, the intensity of this band increases, indicating thermal feeding of the emitting state. In figure 3(*b*), a schematic representation of the excited states dynamics of this system is proposed. The nature of the low energy emission, i.e. the so-called D-band observed in Bi^{3+}-activated wide gap lattices, still constitutes an open question. The most frequently invoked mechanisms imply emission from trapped excitons [30–32] or from Bi^{3+} pairs or clusters [2, 33]. Recently, Boutinaud [19] tentatively ascribed this band to a $Bi^{3+} \rightarrow Y^{3+}$ MMCT transition. His model located the excitation edge at 252 nm in correspondence to the strong Bi^{3+} emission.

On the other hand, concentration dependent emission measurements have not yet been carried out on this material and thus the possible role of Bi^{3+} pairs or clusters has yet to be assessed. The shape of the sideband clearly demonstrates the presence at least two components. At the present state of the investigation, the possibility of having two different processes contributing to this emission cannot be excluded.

3.3. *YVO_4 and YVO_4:Bi^{3+}*

The room temperature excitation and emission spectra of pure, 0.1%, and 1% Bi^{3+}-doped YVO_4 are shown in figures 4(*a*) and (*b*). The excitation edge (evaluated in correspondence with the inflection point of the excitation profile) of pure YVO_4 is at about 335 nm (maximum excitation at 325 nm), and its luminescence spectrum consists of a broadband in the blue region (maximum around 440 nm). The following features are assigned to transitions of the VO_4^{3-} molecular ion: the excitation band to the spin allowed $^1T_1 \leftarrow {}^1A_1$ absorption and the emission to the spin forbidden $^3T_{1,2} \rightarrow {}^1A_1$ transition [34].

The emission spectrum was limited to 400 nm (on the high energy side) because of the working range of the optical filter (UG11) used to eliminate the stray light. However, the vanadate emission band certainly extends to the near UV region and overlaps, at least in part, the excitation band of the Bi^{3+} doped material. This knowledge is important to understand the luminescence dynamics discussed below. The luminescence of YVO_4:Bi^{3+} is extended to the whole visible range, with maximum around 570 nm in the yellow region. The shape of the emission spectrum is independent of the excitation wavelength. However, it is worth noting that the emission maximum of the diluted phosphor is located at a slightly higher energy with respect to the concentrated phosphor and presents an evident shoulder on its low energy side. The excitation edge is significantly shifted towards longer wavelengths with respect to the un-doped compound. Its position depends on the Bi^{3+} concentration, and is located around 345 nm in the diluted sample and around 355 nm in the more concentrated sample. In the frame of a systematic investigation concerning Bi^{3+}-activated lattices [35], we have ascribed these features to transitions involving a metal-to-metal charge transfer state (MMCT) within the bismuth-vanadate complex, which is in general agreement with previous literature [1]. The excited MMCT state results from transitions between Bi^{3+} ($6s^2$)-V^{5+}($3d^0$) and Bi^{4+}($6s^1$)-V^{4+}($3d^1$) configurations. It is also defined as a trapped exciton state or referred to as a D-level state. Its dependence on the Bi^{3+} concentration was theoretically investigated by Dolgos *et al* [36], who concluded that the 6s and 6p orbitals of Bi^{3+} hybridize with the non-bonding and the anti-bonding orbitals of the VO_4^{3-} group, with the effect of a progressive reduction of the bandgap with the doping concentration. Figure 5 shows the low temperature emission spectra of YVO_4:Bi^{3+} (1%) measured upon different excitation wavelengths in high resolution conditions.

It is interesting to note that the MMCT emission presents at least two components with maxima at 550 and 630 nm. Moreover, the 10 K emission profile strongly depends on the

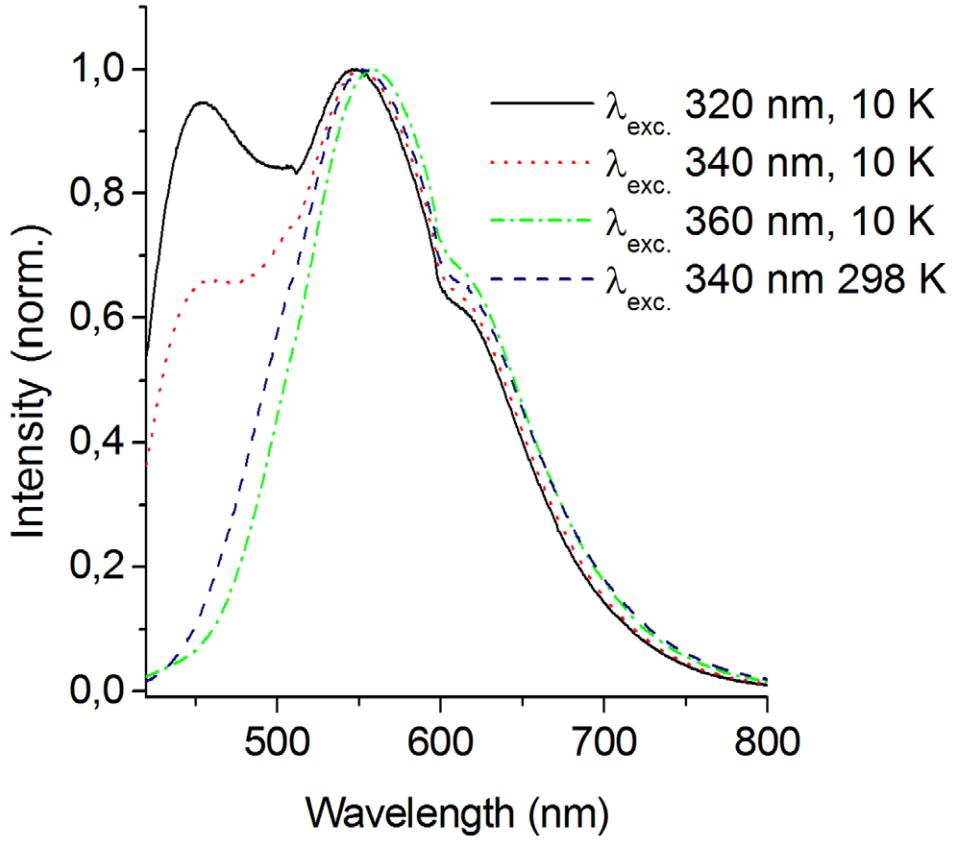

Figure 5. Low temperature emission spectra of $YVO_4:Bi^{3+}$ measured upon different excitation wavelengths. The room temperature spectrum has been added for comparison. The intensities are normalized.

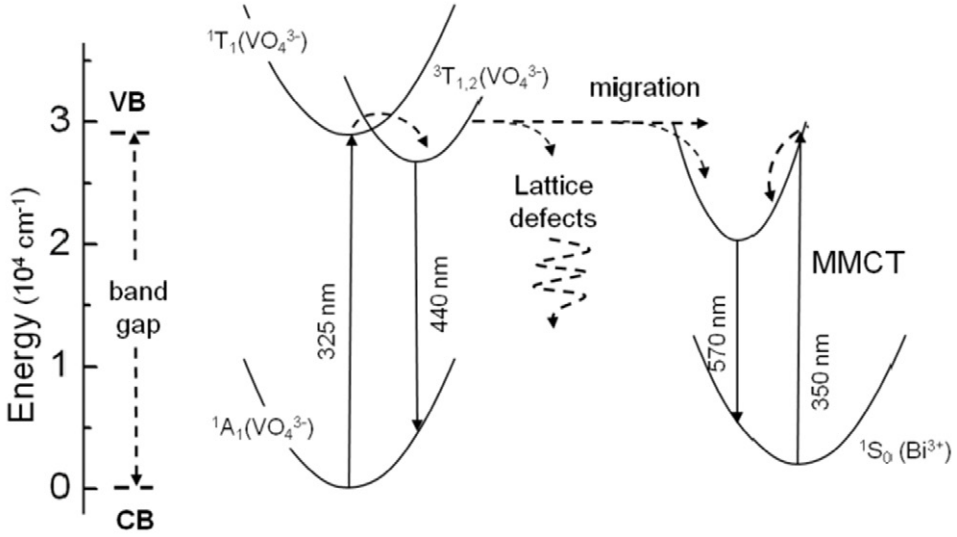

Figure 6. Configurational coordinate diagram illustrating the excited state dynamics of the $YVO_4:Bi^{3+}$ system. The extent of the host bandgap is indicated on the left part as a reference.

excitation conditions, at variance with the room temperature spectrum. In particular, excitation into the vanadate absorption band results in both blue and yellow emissions whereas excitation into the MMCT band (340–360 nm) yields yellow emission only. These results are in partial agreement with those of Moncorgé *et al* [17], who dealt with the temperature behaviour of yellow luminescence for a fixed excitation wavelength (337 nm) only. These observations can be accounted for on the basis of the configurational coordinate diagrams in figure 6.

The excitation of the VO_4^{3-} ion (325 nm, transition $^1T_1 \rightarrow {}^1A_1$) is followed by an intersystem crossing to the triplet states $^3T_{1,2}$ with subsequent blue emission or energy transfer to nearby acceptors. It has been already shown that the host sensitization of yellow emission in $YVO_4:Bi^{3+}$

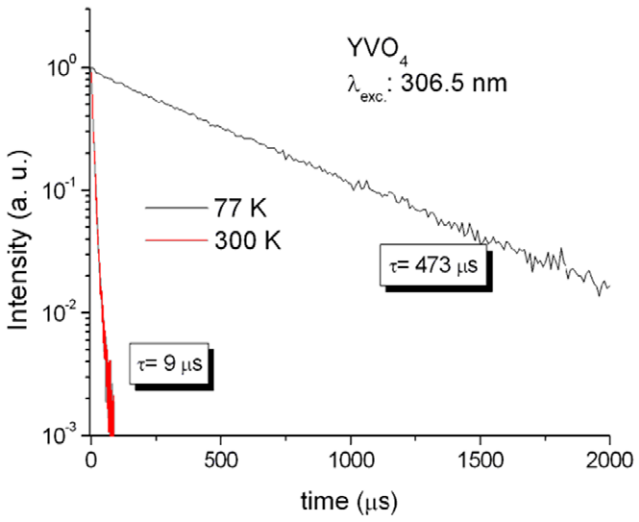

Figure 7. Decay profiles of the host emission.

involves a temperature assisted migration process [17]. As mentioned above, the MMCT state results from the promotion of an electron from the $^1S_0$ ground state configuration of Bi^{3+} to the bottom of the host conduction band. Emission results with a relatively large Stokes shift after lattice relaxation. The application of equation (1) in connection with the data listed in table 2 for $x = 0$ allows the prediction of the MMCT excitation transition at about 330 nm, a reasonable value in consideration of the intrinsic error of the model ($\pm 3000\,cm^{-1}$). We have carried out a series of pulsed light experiments in an attempt to obtain further information on the excitation mechanisms. The decay profile of pure YVO_4 is reported in figure 7: at 77 K it is a single exponential with a decay time of 473 μs whereas at room temperature it is approximately a double exponential whose major, and shorter, component has a decay time of 9 μs. These results indicate strong quenching of the vanadate emission. They are in perfect agreement with those reported by Moncorgé *et al* [17], who proposed an excitonic model including the formation of self- trapped excitons (that can be identified with the vanadate triplet states) and a thermally activated energy migration to radiationless quenching sites (see figure 6).

The decay profiles of YVO_4:Bi^{3+} have been measured upon 306 and 337 nm excitation in the temperature range 77–300 K for two different doping concentrations. Direct pumping into the MMCT band maximum at 337 nm (figure 8(*a*)) results in single exponential, temperature and concentration quasi-independent profiles with decay times of about 4.3 μs, indicating that the emission from the MMCT state is scarcely affected by non-radiative processes.

We checked that the vanadate emission has a negligible contribution under these conditions. These results are in good agreement with those reported by Moncorgé *et al* [17], which supposed that Bi^{3+} induces a distortion of the surrounding vanadate units, creating host traps that can trap the excitons and transfer the energy to their nearby activators. The nature of these activators was not explicitly specified (Bi^{3+} ions, trapped excitons). For this connection, our interpretative scheme based on the formation of the MMCT state clarifies this aspect and is substantially compatible with the analysis carried out in [17]. As a matter of fact, it constitutes a significant evolution of the previously proposed model and is supported by a systematic study [19] and new experimental results. Upon excitation at 306.5 nm, the MMCT emission exhibits very different decays as a function of temperature. At room temperature (figure 8(*b*)), the profiles are exponential with a time-constant of 5.5 μs and present a build-up. The rise time is shorter (0.42 μs) for YVO_4:1%Bi^{3+} and longer (0.69 μs) for YVO_4:0.1%Bi^{3+}. These results confirm that the MMCT state is fed by energy transfer from the host excited states. At 77 K, the migration process is hampered. The decay curves consist of the sum of a long and a short lived component (figure 8(*c*)). The long lived component has a time constant ranging from 413 μs in YVO_4:1%Bi^{3+} to 446 μs in YVO_4:0.1%Bi^{3+}. This component is ascribed to the VO_4^{3-} emission that is not quenched at this temperature and has some contribution at 520 nm. The short lived component is ascribed to the MMCT emission and is mostly induced by direct energy transfer from the nearest neighbour excited vanadate ions. Figure 8(*d*) shows the decay profiles of the vanadate emission observed in YVO_4:Bi^{3+} upon excitation at 306.5 nm. At 77 K, the decay is exponential with a time constant close to that of the un-doped compound. At 295 K (inset of figure 8(*d*)), the decay becomes strongly non-exponential with a time constant much shorter than in un-doped YVO_4. This confirms that part of the energy absorbed by the host is transported by migration to Bi^{3+} ions only when the temperature is higher than 77 K. Measurements carried out on single crystals provide further information on the emission mechanism. The room temperature excitation and emission spectra of YVO_4:Bi crystals are shown in figure 9(*a*) and are rather similar to those of the powder sample. However, at low temperatures (figure 9(*b*)), their behaviour is different from that observed in figure 5 since the vanadate emission is only barely observable in the 320 nm excited spectrum.

It is evident that the influence of temperature is more pronounced in the powder (figure 10(*a*)) than in the crystal (figure 10(*b*)) sample. We also measured the emission spectra of $YP_{0.99}V_{0.01}O_4$ crystals as a function of temperature (figure 10(*c*)) to verify if the isolated vanadate ion contributes to thermal quenching: the results clearly demonstrate that this possibility can be excluded, which is consistent with the observations of G. Blasse [37, 38], who reported a quenching temperature of 720 K for this material. This means that the energy migration process feeding the MMCT state is much more efficient in the crystals than in the powders. We further investigated this interesting aspect by measuring the temperature dependence of the VO_4^{3-} emission intensity of un-doped crystals and powders. The results are summarized in figure 10.

The observed trends were reproduced using a model proposed by Boulon *et al* [39].

$$\frac{I(T)}{I_0} = \left[1 + C\exp\left(-\frac{\Delta E}{kT}\right)\right]^{-1} \qquad (2)$$

where C is a constant and ΔE represents the activation energy for the migration process among the vanadate triplet states. It

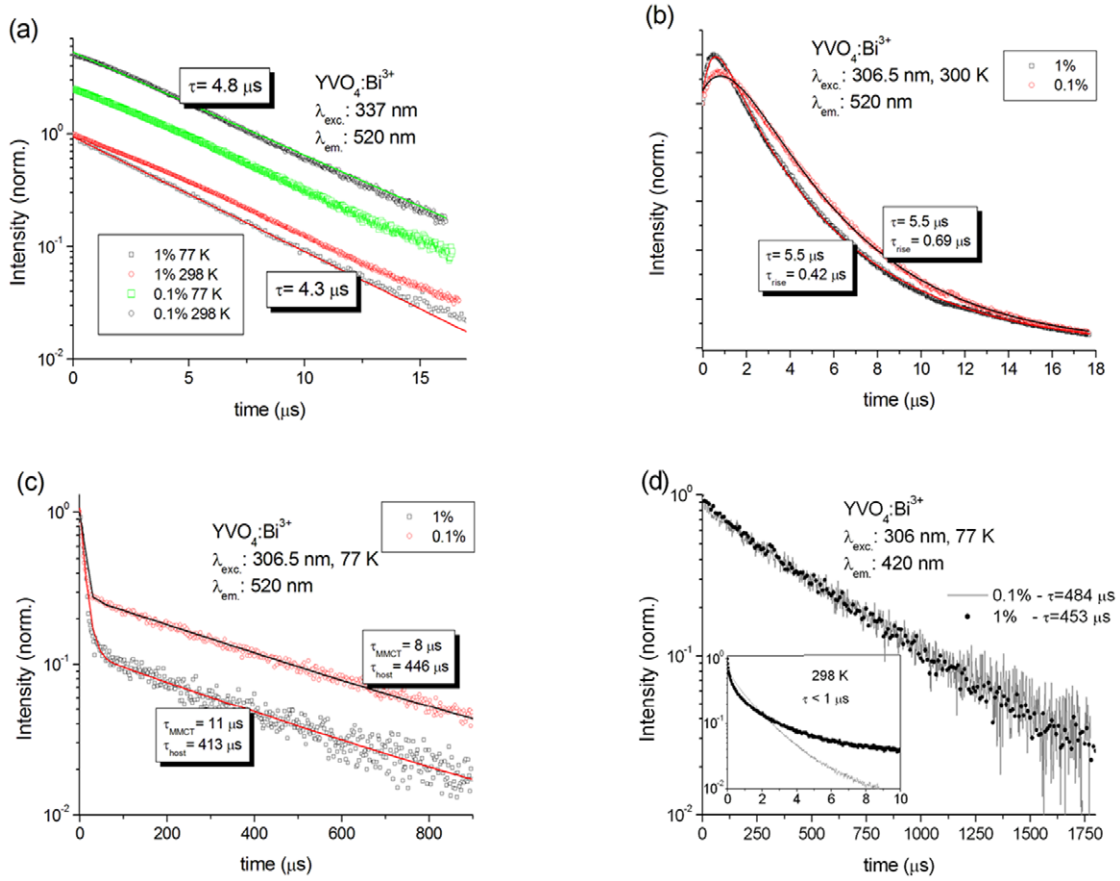

Figure 8. (*a*) Decay profiles of the yellow emission measured upon MMCT excitation. Full line: single exponential fit; (*b*) room temperature decay profiles of the yellow emission measured upon host excitation. Full line: fit with difference of exponential function; (*c*) low temperature decay profiles of the yellow emission measured upon host excitation. Full line: double exponential fit; (*d*) low temperature decay profiles of the blue emission measured upon host excitation. The profiles measured at room temperature are shown in the inset.

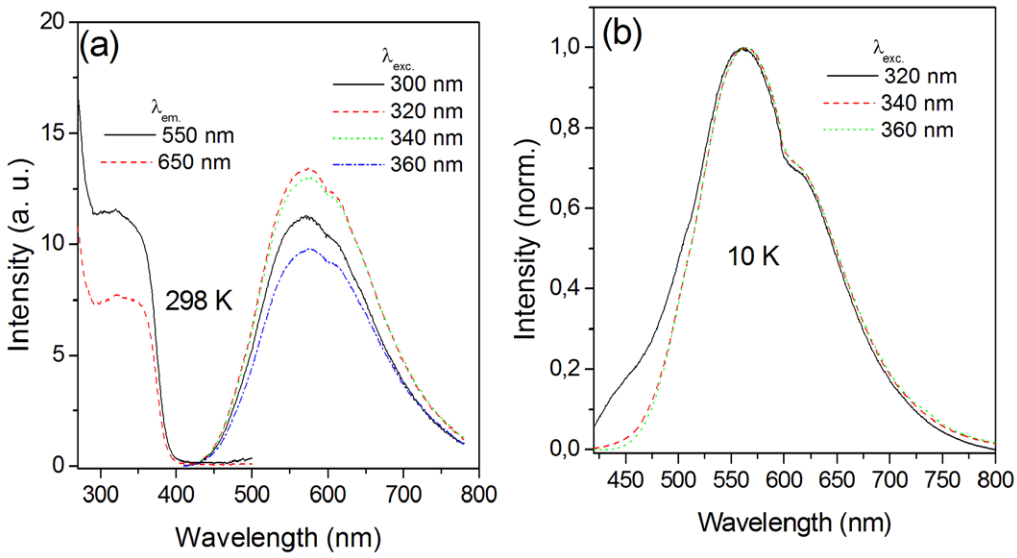

Figure 9. Emission properties of $YVO_4:Bi^{3+}$ crystals. (*a*) 298 K excitation and emission spectra. (*b*) 10 K emission spectra (normalized with respect to the maximum).

should be pointed out that its value is significantly lower in for crystals than for powders. These results are fully consistent with those shown in figure 9 and confirm the role of the migration process in the dynamics of this system. It is also interesting to note the shift of the emission maximum from 440 nm at 10 K to 460 nm at 298 K. According to Blasse [37],

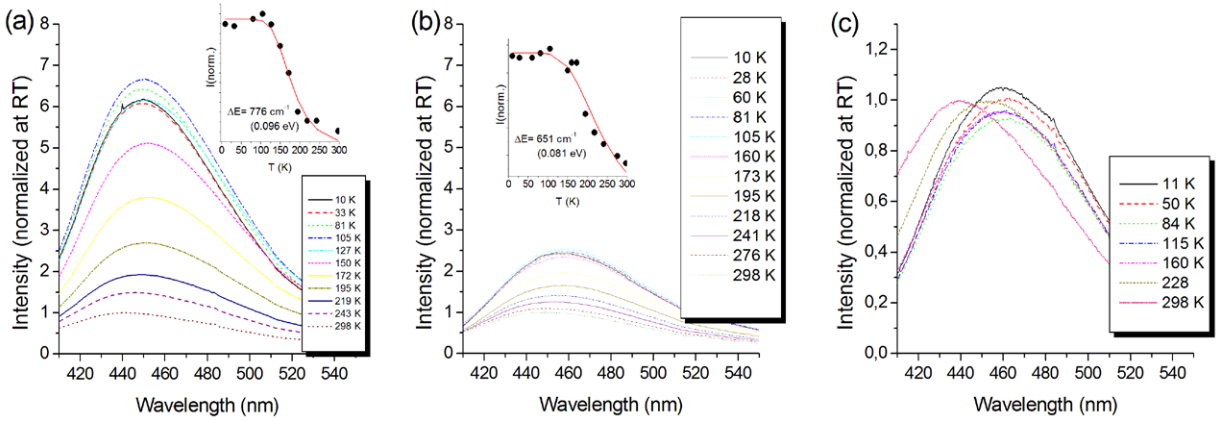

Figure 10. Temperature dependence of the 340 nm excited emission of pure YVO_4 powders (*a*) and crystals (*b*) and of $YP_{0.99}V_{0.01}O_4$ crystals (excitation at 290 nm) (*c*). The spectra are normalized with respect to the room temperature emission. The intensity trends are shown in the insets. The full lines correspond to the fitted curves calculated using equation (2).

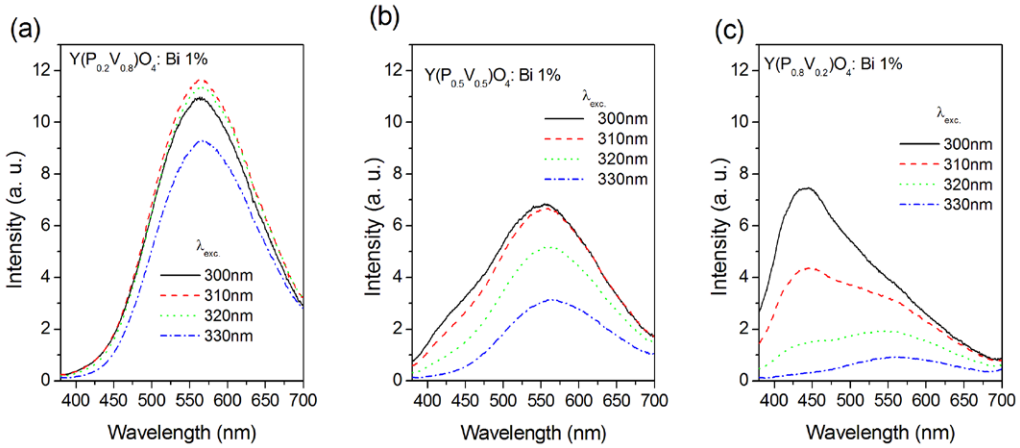

Figure 11. Room temperature emission spectra of $Y(P_xV_{1-x})O_4:Bi^{3+}$ (1%). (*a*) $x = 0.2$; (*b*) $x = 0.5$; (*c*) $x = 0.8$. The intensity scale is the same for all spectra for the sake of comparison.

this can be ascribed to the thermal population of the $^3T_2$ excited level, located around 1040 cm^{-1} above the $^3T_1$ lowest lying emitting state.

3.4. $Y(P_xV_{1-x})O_4:Bi^{3+}$

The 298 K luminescence spectra along the $Y(P_xV_{1-x})O_4:Bi^{3+}$ (1%) (x = 0.2, 0.5, 0.8) compositions were measured upon different excitation wavelengths and are shown in figure 11.

For $x = 0.2$ (figure 11(*a*)), the observed behaviour is practically identical to that of $YVO_4:Bi^{3+}$. For $x = 0.5$ (figure 11(*b*)), the appearance of an incipient blue component can be discerned in the emission spectra excited at wavelengths shorter than 320 nm, i.e. upon host excitation. For x = 0.8 (figure 11(*c*)), the emission properties are strongly dependent on the excitation wavelength: the intensity ratio between the blue and the yellow band as well as the overall emission intensity strongly decrease on moving from the host to MMCT excitation. In this phosphor, the migration process is strongly limited by the large distance between the VO_4^{3-} units. As a consequence, the luminescence properties are essentially regulated by direct excitation and energy transfer processes occurring between isolated centres. The emission spectra in figure 12 were collected at 10 K with the high resolution setup for $x = 0.5$ and $x = 0.8$.

The results confirm that the vanadate sensitization of Bi^{3+} luminescence occurs through a thermally assisted migration process. We further note that the maximum of MMCT emission undergoes a red shift:

(i) as the excitation wavelength is increased, for fixed composition and temperature;
(ii) on passing from x = 0 (maximum at 558 nm, figure 5) to x = 0.8 (maximum at 573 nm, figure 12), for a given excitation wavelength and fixed temperature;
(iii) as the temperature decreases, for fixed composition and excitation wavelength.

This red shift is due to an increment of the relative contribution of the 630 nm component and is roughly proportional to the P content x. In figure 13, the room temperature excitation spectra are reported as a function of the host composition. The excitation edge undergoes a blue shift from ≈355 to ≈315 nm as V is substituted by P. This behaviour is accounted for in the next section.

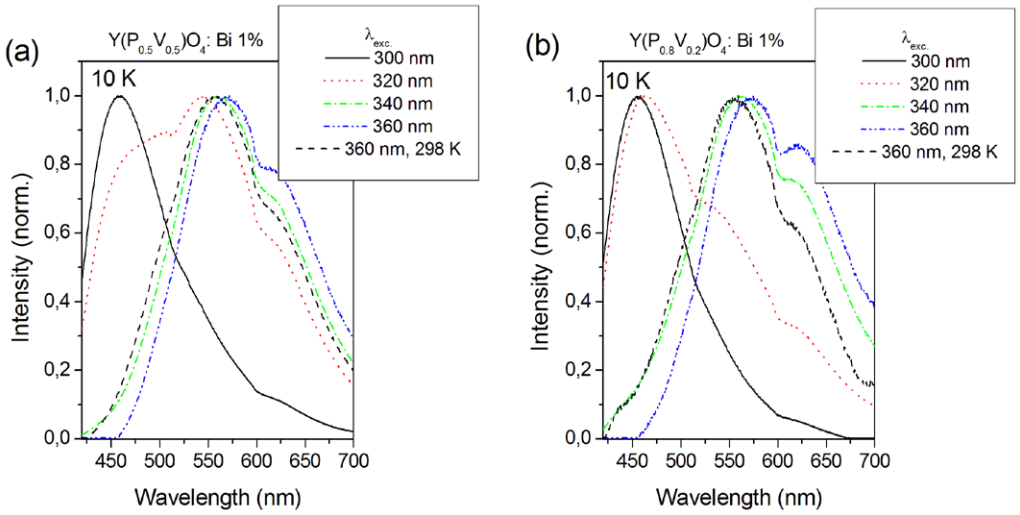

Figure 12. Low temperature emission spectra of $Y(P_xV_{1-x})O_4:Bi^{3+}$ (1%). (*a*) $x = 0.5$; (*b*) $x = 0.8$. The intensities are normalized.

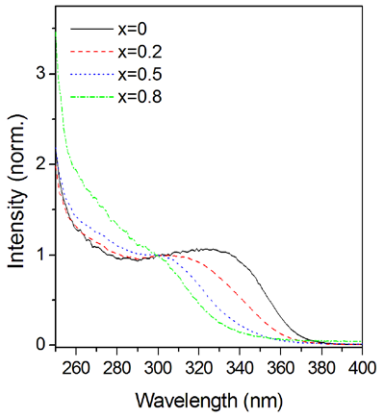

Figure 13. Room temperature excitation spectra of $Y(P_xV_{1-x})O_4:Bi^{3+}$ (1%) ($\lambda_{em.}$: 550 nm).

The decay curves for the two components of MMCT emission monitored at 520 and 660 nm upon excitation at 337 nm are shown in figure 14(*a*) for the composition $YP_{0.8}V_{0.2}O_4$:1%Bi^{3+}.

The decay curves are nearly single exponential and the decay times, 4.6 μs for the 550 nm and 4.0 μs for the 630 nm band, are rather similar; this is consistent with the fact that they have the same nature. The decay profiles of the host vanadate emission were measured in the same compound at 300 and 77 K, upon 306 nm excitation (figure 14(*b*)). Both are nearly single exponential, with decay times (195 and 830 μs) much longer than that of the pure vanadate host. This effect is obviously a consequence of the fact that the migration of the excitation is strongly inhibited in this host lattice.

3.5. Discussion and DFT calculations

The DFT calculations carried out as a function of the host composition provide assistance in the interpretation of some spectroscopic observations. The results are summarized in figure 15, where the DOS diagrams calculated for the pure and mixed $YV_{1-x}P_xO_4$ ($x = 0$; 0.25; 0.5; 0.75; 1.0) compounds are shown. It can be seen that the conduction band of YPO_4 is considerably wider than that of YVO_4 due to the interaction between the Y 4d and P 3p orbitals. The P 3p orbitals produce a minor (compared to the Y 3d states) contribution at the upper part of the conduction band, which otherwise has a predominantly Y 3d character. The width and structure of the valence band also changes when passing from YVO_4 to YPO_4. The P 3p states are localized at the valence band bottom and are separated by a narrow gap from the O 2p states, which make up the upper and wider part of the valence band. The MMCT transition is associated with an excitation from the Bi^{3+} ground state to the conduction band of the host material. Its energy then depends (i) on the position of the Bi^{3+} electronic levels within the host bandgap and (ii) on the extension of the bandgap. The first aspect is related to the interaction of the Bi^{3+} 6s and 6p orbitals with the 2p orbitals of the surroundings oxygen ligands. It has already been observed that this interaction induces the concentration dependence of the excitation edge observed in figure 4(*a*). When the doping level is kept constant, we consider it reasonable to ascribe the shift of the excitation edge (observed in figure 13) to the progressive increase of the host bandgap (from 2.8 to 5 eV) that takes place as P replaces V, referred to as gap bowing.

DFT calculations are consistent with this hypothesis; even though the estimated values are systematically lower than the experimental values (typical of DFT calculations), the trend is nevertheless consistent with the behaviour observed in figure 13 since the calculated value of the total shift (2930 cm^{-1}) is not very different from the measured value (3200 cm^{-1}). Another relevant aspect concerns the conduction band of YPO_4; it is mainly constituted of the d orbitals of Y^{3+}. This is consistent with the assignment of the $YPO_4:Bi^{3+}$ D band to an MMCT transition from Bi to Y proposed in [19].

3.6. Colour measurements and quantum yields

We measured the colour coordinates and the internal quantum yields (i.e. the ratio between the integrated intensities of the absorbed and emitted radiation) of the title materials for

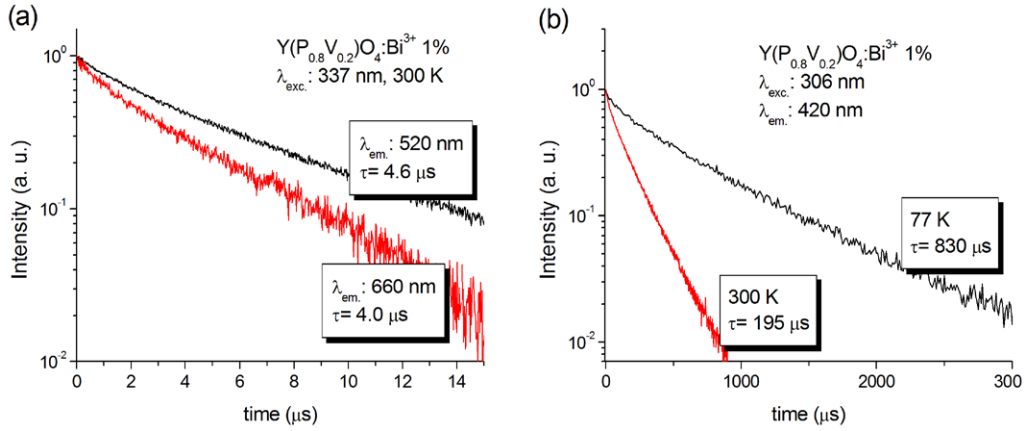

Figure 14. Decay profiles of the $Y(P_{0.8}V_{0.2})O_4:Bi^{3+}$ (1%) emission upon MMCT excitation (*a*) and host excitation (*b*).

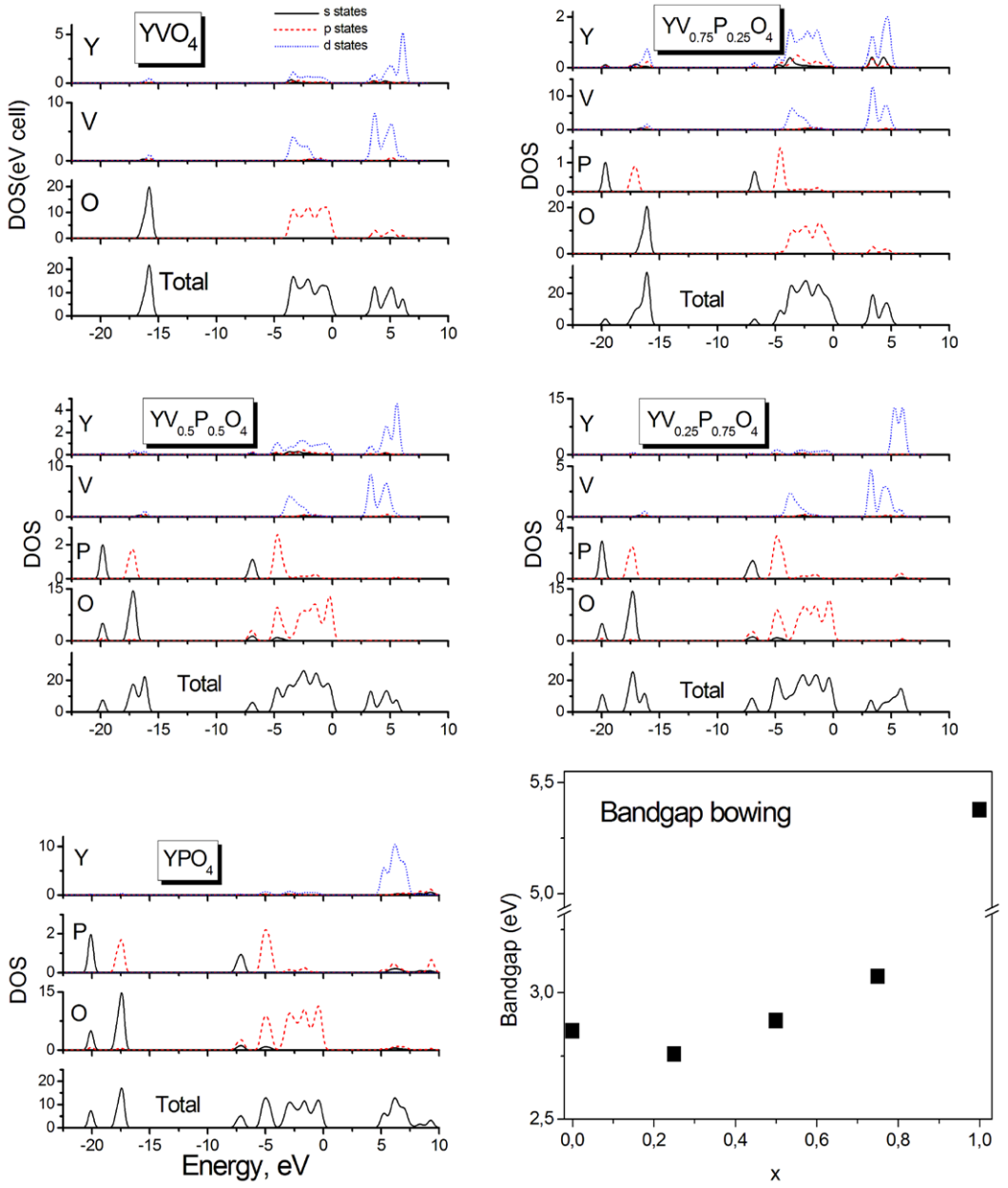

Figure 15. Calculated DOS and bandgap bowing for $YV_{1-x}P_xO_4$ ($x = 0$; 0.25; 0.5; 0.75; 1.0).

Table 3. Colour coordinates and internal quantum yield along the $Y(P_xV_{1-x})O_4:Bi^{3+}$ 1% series as a function of the excitation wavelength. The format is: X, Y (IQY), where X and Y are the colour coordinates (CIE 1931) and IQY the internal quantum yield.

x	λ_{exc} = 290 nm	λ_{exc} = 300 nm	λ_{exc} = 310 nm	λ_{exc} = 320 nm
0	0.401, 0.479 (0.753)	0.403, 0.480 (0.881)	0.405, 0.482 (0.924)	0.408, 0.483 (0.929)
0.2	0.391, 0.471 (0.798)	0.391, 0.470 (0.885)	0.393, 0.471 (0.892)	0.397, 0474 (0.822)
0.5	0.335, 0.402 (0.650)	0.339, 0.407 (0.702)	0.349, 0.419 (0.641)	0.366, 0.438 (0.466)
0.6	0.295, 0.343 (0.686)	0.302, 0.351 (0.729)	0.320, 0.375 (0.656)	0.345, 0.405 (0.481)
0.7	0.262, 0.295 (0.613)	0.271, 0.308 (0.588)	0.289, 0.333 (0.459)	0.319, 0.372 (0.238)
0.8	0.224, 0.236 (0.540)	0.236, 0.255 (0.507)	0.260, 0.291 (0.353)	0.301, 0.345 (0.177)

different excitation wavelengths in the range 290–320 nm. The results are summarized in table 3.

It is worth noting that the internal quantum yield significantly decreases on passing from $x = 0$ to $x = 0.8$, again demonstrating the role of the migration in the luminescence process.

In agreement with the emission spectra, the colour coordinates are nearly independent of the excitation wavelength for low x values, 0 and 0.2. As x increases, dependence of the emitted colour on the excitation wavelength progressively increases, as evidenced in figure 16(*a*). The colour of the luminescence ranges from blue to yellow depending on the composition and the excitation wavelength. For example, figure 16(*b*) shows the luminescence along the phosphor series upon 254 nm lamp excitation. We believe that the developed materials have interesting device potentialities thanks to their versatility and efficiency.

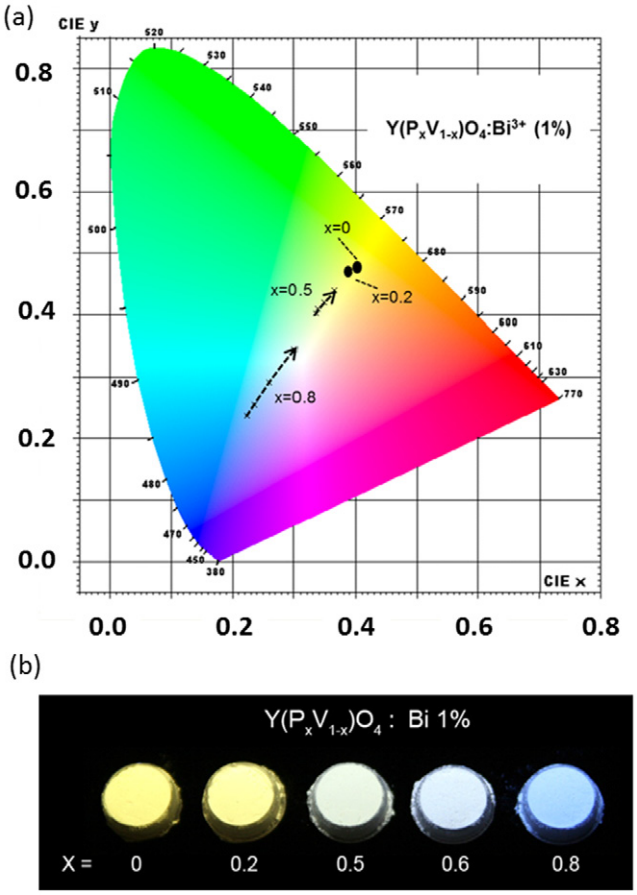

Figure 16. (*a*) Chromaticity diagram showing the colour coordinates of the investigated materials and their evolution with the increasing excitation wavelength (see table 1). (*b*) Luminescence along the phosphor series upon 254 nm lamp excitation.

4. Concluding remarks

The emission spectrum of $YPO_4:Bi^{3+}$ presents an intense transition at 245 nm and a weaker and broader feature around 335 nm. In a number of studies on Bi^{3+}-doped into wide bandgap hosts, a similar emission was interpreted as the radiative decay of a localized charge transfer state arising from a photoionization process in which the luminescent centre ejects an electron into the host lattice conduction band [30–32]. This results in the formation of an impurity bound exciton state in which the electron is delocalized in the host lattice and the hole is trapped at the luminescent centre. The analogy with the MMCT model proposed to account for the yellow $YVO_4:Bi^{3+}$ luminescence is rather evident, even if the two cases present important differences. The bandgap of YPO_4 is, in fact, around 9.2 eV whereas that of YVO_4 is of the order of 4.2 eV [13]. The excited levels of Bi^{3+} are presumably located within the host band gap in the former case and in the conduction band in the latter. As a consequence, Bi^{3+} excitation results in $^3P_1$ emission in the phosphate as well as a photoionisation process involving the formation of an MMCT state in the vanadate lattice. Moreover, for the phosphate, it is not possible to exclude the possibility of interaction between Bi^{3+} ions located at sufficiently short distances to generate pair- or cluster-related excited states. This aspect must be carefully verified before proceeding to a definite assignment of the lower energy emission feature. In $YVO_4:Bi^{3+}$, the MMCT state can be efficiently populated upon host excitation through energy migration. The dependence of this process on temperature, host composition, and morphology has been thoroughly investigated as well as the structure of the visible emission, which has never been reported nor discussed up to now, as far as we know, and whose origin is unclear. The intensity ratio between the 550 and 630 nm components depends on the host composition, inducing in turn a progressive dependence on temperature and the excitation wavelength. This does not appear to be compatible with a splitting of the excited state induced by site symmetry and/or the Jahn-Teller effect or with the sample defectiveness, which does not depend on the composition. We have also considered the possibility of the formation of two different MMCT states is connected to the fact that the second coordination sphere of Y^{3+} (and then of Bi^{3+}) consists of two different kinds of $P^{5+}(V^{5+})$ ions located at distances

of 3.01–3.15 Å (2 ions, axial position) and 3.75–3.89 Å (four ions, compressed tetrahedral arrangement) (figure 1(*c*) and table 2). However, this model does not account for all experimental observations and the agreement with equation (1) is only qualitative. Supplementary measurements, e.g. the excited state EPR, could be of assistance in elucidating this point. Finally, the emission performance of the developed materials was measured to provide useful information in view of technological applications.

Acknowledgements

M G B acknowledges financial support from Marie Curie Initial Training Network LUMINET (Grant Agreement 316906). We also wish to acknowledge Dr G A Kumar (University of Texas at San Antonio) for allowing us to use the Materials Studio package.

References

[1] Blasse G and Bril A 1968 *J. Chem. Phys*. **48** 217–22
[2] Setlur A A and Srivastava A M 2006 *Opt. Mater*. **29** 410–5
[3] Blasse G and van der Steen A C 1979 *Solid State Commun*. **31** 993–4
[4] Mu Z, Hu Y, Chen L and Wang X 2011 *J. Lumin*. **131** 1687–91
[5] Zeng X, Im S-J, Jang S-H, Kim Y-M, Park H-B, Son S-H, Hatanaka H, Kim G-Y and Kim S-G 2006 *J. Lumin*. **121** 1–6
[6] Jia W, Perez-Andújar A and Rivera I 2003 *J. Electrochem. Soc*. **150** H161–4
[7] He Y, Zhao M, Song Y, Zhao G and Ai X 2011 *J. Lumin*. **131** 1144–8
[8] Xia Z, Chen D, Yang M and Ying T 2010 *J. Phys. Chem. Solids* **71** 175–80
[9] Sun J, Xian J, Xia Z and Du H 2010 *J. Lumin*. **130** 1818–24
[10] Bos A J J, Dorenbos P, Bessière A and Viana B 2008 *Radiat. Meas*. **43** 222–6
[11] Kaminskii A A, Bettinelli M, Speghini A, Rher H, Eichler H J and Mariotto G 2008 *Laser Phys. Lett*. **5** 367–74
[12] Miller S A, Caspers H H and Rast H E 1968 *Phys. Rev.* **168** 964–9
[13] Dorenbos P, Krumpel A H, van der Kolk E, Boutinaud P, Bettinelli M and Cavalli E 2010 *Opt. Mater*. **32** 1681–5
[14] Guillot-Noel O, Bellamy B, Viana B and Gourier D 1999 *Phys. Rev B* **60** 1668–77
[15] van de Craats A M and Blasse G 1996 *Mat. Res. Bull*. **31** 381–7
[16] Jüstel T, Huppertz P, Mayr W and Wiechert D U 2004 *J. Lumin*. **106** 225–33
[17] Moncorgé R and Boulon G 1979 *J. Lumin*. **18–19** 376–80
[18] Li J, Liu J and Yu X 2011 *J. Alloys Compounds* **509** 9897–900
[19] Boutinaud P 2013 *Inorg. Chem.* **52** 6028–38
[20] Angiuli F, Mezzadri F and Cavalli E 2011 *J. Solid State Chem*. **184** 1843–9
[21] Angiuli F, Cavalli E and Belletti A 2012 *J. Solid State Chem*. **192** 289–95
[22] Garton G, Smith S H and Wanklyn B M 1972 *J. Cryst. Growth* **13–14** 588–92
[23] Hazenkamp M, Stückl A C, Cavalli E and Güdel H U 2000 *Inorg. Chem*. **39** 251–4
[24] Clark S J, Segall M D, Pickard C J, Hasnip P J, Probert M J, Refson K and Payne M C 2005 *Z. Kristallogr*. **220** 567–70
[25] Ropp R C and Carrol B 1973 *J. Inorg. Nucl. Chem*. **35** 1153–7
[26] Pan G, Song H, Dai Q, Qin R, Bai X, Dong B, Fan L and Wang F 2008 *J. Appl. Phys.* **104**, 084910
[27] Ropp R C and Carrol B 1975 *Inorg. Chem*. **14** 2199–202 and references therein
[28] Momma K and Izumi F 2008 *J. Appl. Crystallogr*. **41** 653–8
[29] Babin V, Gorbenko V, Krasnikov A, Makhov A, Nikl M, Zazubovich S and Zorenko Y 2010 *Radiat. Meas*. **45** 331–5
[30] Srivastava A M and Beers W W 1999 *J. Lumin*. **81** 293–300
[31] Blasse G, de Mello Donega C, Berezovskaya I and Dotsenko V 1994 *Solid State Commun.* **91** 29–31
[32] Dotsenko V P, Berezovskaya I V and Efryushina N P 1996 *J. Phys. Chem. Solids* **57** 437–41
[33] Srivastava A M 2002 *Mater. Res. Bull*. **37** 745–51
[34] Barendswaard W, Weber R T and van der Waals J H 1987 *J. Chem. Phys*. **87** 3731–8
[35] Boutinaud P and Cavalli E 2011 *Chem. Phys. Lett*. **503** 239–43
[36] Dolgos M R, Paraskos A M, Stoltzfus M W, Yarnell S C and Woodward P M 2009 *J. Solid State Chem*. **182** 1964–71
[37] Blasse G 1980 *Struct. Bond*. **42** 1–41
[38] Blasse G 1968 *Philips Res. Rep.* **23** 344–61
[39] Boulon G, Gaume-Mahn F and Curie D 1970 *C. R. Acad. Sci. Paris B* **270** 111–4